Electronic supplementary information

Synthetic loose-packed monoclinic $BiVO_4$ nanoellipsoids with novel multiresponses to visible light, trace gas and temperature

Yongfu Sun, Changzheng Wu, Ran Long, Yang Cui, Shudong Zhang and Yi Xie*

Hefei National Laboratory for Physical Sciences at Microscale,
University of Science & Technology of China, Hefei, 230026, P.R. China.
Fax: 86-551-3603987, E-mail: yxie@ustc.edu.cn

S1. Experimental

Preparation: In a typical synthesis, 15 mmol NaOH was added to a solution of 10 mL oleic acid in 20 mL ethanol. Then a solution of $Bi(NO_3)_3{\cdot}5H_2O$ (5 mL H_2O, 0.4 mL 36% HCl, 0.04 mol L^{-1}) and an aqueous solution of $Na_3VO_4{\cdot}12H_2O$ (5 mL H_2O, 0.04 mol L^{-1}) were added to the above mixture. After stirring for a while, the mixture was transferred into a stainless Teflon-lined 50 mL-capacity autoclave, which was sealed and maintained at 100 °C for 6 h. The system was allowed to cool to room temperature and then final products spontaneously separated at the bottom of the autoclave. For comparison, we also prepared bulk $BiVO_4$ powders by traditional solid state reaction according to Ref. [1]. That is to say, after mixing starting materials of $Bi(NO_3)_3{\cdot}5H_2O$ and NH_4VO_3, the powders were dried at 120 °C for 24 h, and then were grinded and calcined at 700 °C for 8 h.

Characterization and measurements: XRD patterns were recorded by using a Philips X'Pert Pro Super diffractometer with Cu Kα radiation (λ = 1.54178 Å), FESEM was performed by using an FEI Sirion-200 SEM, the TEM and HRTEM images associated with SAED analyses were performed by using a JEOL-2010 TEM with an acceleration voltage of 200 kV. X-ray photoelectron spectra (XPS) was acquired on an ESCALAB MKII with Mg Kα (hυ = 1253.6 eV) as the excitation source. The binding energies obtained in the XPS spectral analysis were corrected for specimen charging by referencing C 1s to 284.5 eV. Raman spectra were detected by a RenishawRM3000 Micro-Raman system. The Brunaure-Emmett-Teller (BET) surface area was determined by nitrogen adsorption (Micromeritices ASAP 2000 system). The photocatalytic performance of ellipsoidal $BiVO_4$ was evaluated by the photodegradation of RB under visible-light irradiation, which was provided by a Xenon lamp with a 380 nm cut-off filter. An aqueous suspension of $BiVO_4$ was prepared by adding powered $BiVO_4$ (0.6 mmol) to an aqueous solution of RB (100 ml, 10^{-5} M). The solution was protected from light and stirred for 6 h to reach adsorption equilibrium and uniform dispersion and then was exposed to visible light irradiation. Concentrations of RB were carried out using UV/Vis-NIR spectrophotometer (Shimadzu SolidSpec-3700DUV) every 15 min. The above same procedures were performed for the references of bulk $BiVO_4$ and TiO_2. Gas sensing measurements were performed at room temperature with a WS-30A system (Weisheng Instruments, Zhengzhou, China). DSC cycling curves were measured by the NETZSCH DSC 200 F3 with a heating/cooling rate of 10 °C min^{-1} between 20 °C and 480 °C. Variable temperature XRD patterns of the samples were recorded by the Shimadzu XRD-7000 with Cu Kα radiation (λ = 1.54178 Å).

S2. Characterization of the as-obtained loose-packed m-$BiVO_4$ nanoellipsoids

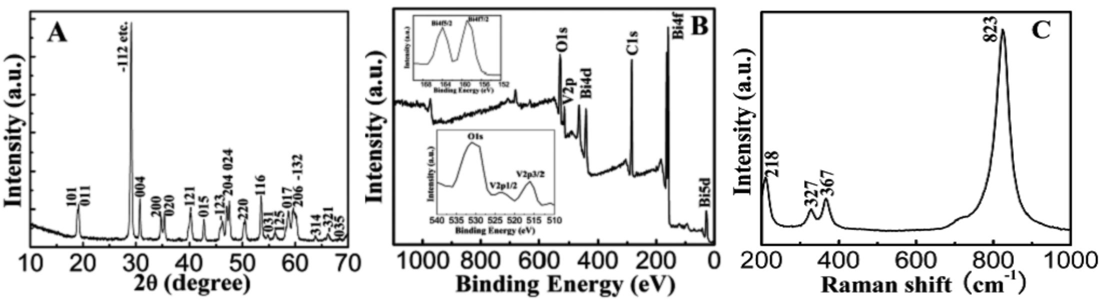

Fig. S1 XRD pattern (A), XPS survey spectra (B) and Raman spectroscopy (C) of the as-obtained product at 100 °C for 6 h

The phase, chemical composition and local structure information for the as-obtained product can be revealed by the X-ray powder diffraction (XRD), X-ray photoelectron spectroscopy (XPS) and Raman spectroscopy, respectively. Thus, as shown in **Fig. S1A**, the XRD pattern of the sample obtained at 100 °C for 6 h could be readily indexed to be a pure monoclinic scheelite $BiVO_4$ (JCPDS card 75-2480). Moreover, XPS analysis provided additional insights into the chemical composition of the synthesized $BiVO_4$ product. Apparently, the characteristic spin-orbit split of the Bi4f5/2 and Bi4f7/2 signals (top inset in **Fig. S1B**), V2p1/2 and V2p3/2 signals (bottom inset in **Fig. S1B**) and also the binding energies of the different elements could be attributed to the typical monoclinic scheelite $BiVO_4$.[2] In this respect, the observed O1s peak at 529.8 eV could be ascribed to the lattice oxygen in crystalline $BiVO_4$.[3] Besides, the average atomic ratio of Bi and V was approximately 1.14 : 1 on the basis of the quantification of Bi4f and V2p peaks, which was consistent with the stoichiometric ratio of $BiVO_4$. Furthermore, Raman scattering spectra of the prepared sample, as shown in **Fig. S1C**, was performed to probe its local structure. In this regard, the 218 cm^{-1} band was the external mode of $BiVO_4$, which gave little structure information. The Raman bands at 327 and 367 cm^{-1} were assigned to the asymmetric and symmetric deformation modes of the VO_4^{3-} tetrahedron, respectively. Meanwhile, the most intense Raman band at about 823 cm^{-1} was assigned to the symmetric V-O stretching mode, while the weak shoulder at about 712 cm^{-1} was assigned to antisymmetric V-O stretch. All these results demonstrated that a pure monoclinic scheelite $BiVO_4$ was successfully synthesized through a mild solvothermal method based on an oleic acid/ethanol/water system.

S3. Optical absorption edges and RB degradation rate under visible-light irradiation of loose-packed m-$BiVO_4$ nanoellipsoids

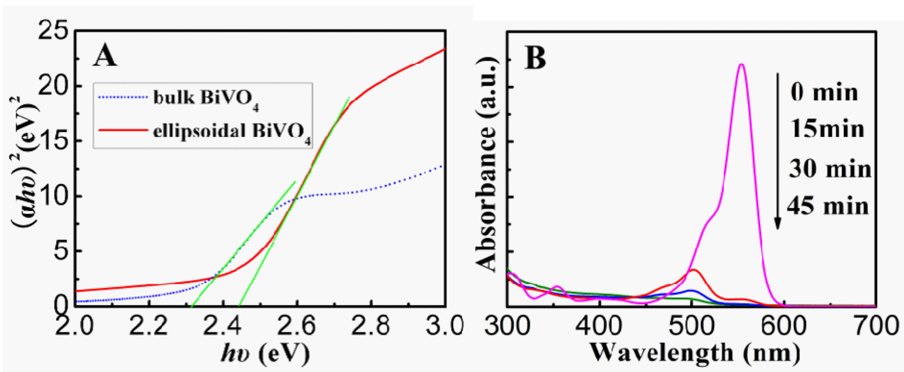

Fig. S2 (A) Optical absorption edges of ellipsoidal and bulk $BiVO_4$: plots of $(\alpha h\nu)^2$ vs. photon energy ($h\nu$). (B) Changes of UV-vis spectra of ellipsoidal $BiVO_4$ suspended RhB solution as a function of irradiation time (λ > 400 nm).

Fig. S2A showed the optical absorption edges (in eV) of ellipsoidal and bulk $BiVO_4$. The band gap energies were, estimated from the $(\alpha h\upsilon)^2$ versus photon energy plots, to be 2.44 eV and 2.31 eV for ellipsoidal and bulk $BiVO_4$, respectively. Obviously, the optical adsorption edge and the band energy of ellipsoidal $BiVO_4$ were blue-shifted in comparison with that of bulk $BiVO_4$, which may be ascribed to the decrease of crystal size of ellipsoidal $BiVO_4$.[2,4]

The photocatalytic performance of ellipsoidal $BiVO_4$ was examined in terms of photodegradation of N,N,N',N'-tetraethylated rhodamine B (RB) under visible-light irradiation. That is to say, RB with a major absorption band at 553 nm was chosen as a model organic pollutant to study the pollutant degradation activities of $BiVO_4$. As shown in **Fig. S2B**, absorption of RB/$BiVO_4$ suspension gradually decreased during the photodegradation under visible-light irradiation. In addition, the major absorption band shift from 553 to 496 nm step by step, indicating removal of ethyl groups one by one. At the same time, the color of the suspension changed gradually, demonstrating that the chromophoric structure of the dye is destroyed.[5]

S4. Sensing mechanism to trace gas of loose-packed m-$BiVO_4$ nanoellipsoids

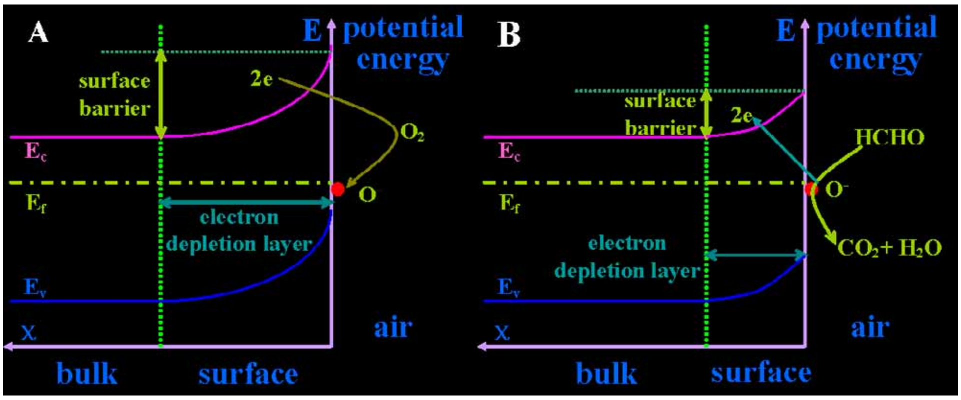

Fig. S3 (A) and (B) Schematic diagrams of the proposed reaction mechanism of m-$BiVO_4$ based sensors to HCHO on the particle's surface

Of note, the principle of the resistance-type sensors is based on the conductance variation of the sensing material, which depends strongly on its surface gas atmosphere exposed to the tested gas. In other words, with regard to the sensing mechanism of $BiVO_4$-based sensors, the adsorption/desorption phenomena and reactions of the gas molecules on the surface of the $BiVO_4$ structure would change its electron-depleted layers and band structures near the surface thus resulting in variation of the resistances.[6-8] Then, the sensing mechanism of m-$BiVO_4$ based sensors was presented in **Fig. S3A** and **B**. As was known, the most important specie adsorbed on their surfaces was oxygen when operating in ambient air. Thus, as shown in **Fig. S3A**, oxygen species were first adsorbed on the surface of m-$BiVO_4$ based sensors in air, and then were ionized into O^- or O_2^- by trapping free electrons from the conduction band of $BiVO_4$ due to the strong electron negativity of the oxygen atom.[9,10] Simultaneously, the decrease of electrons in the conduction band would thicken the electron-depleted layer and increase the surface barrier, thus resulting in a high resistance. In parallel, as depicted in **Fig. S3B**, when the sensor was put into a tested gas, for example formaldehyde in our case, HCHO would be oxidized by O^- or O_2^- to form CO_2 and H_2O.[11] Once the oxidation reaction occurred, electrons trapped by the adsorbed oxygen would return back to the conduction band of $BiVO_4$, which then thinned the electron-depleted layer and decreased the surface barrier, thus resulting in a decrease of the resistance. Therefore, the variations of the resistances in air and in tested gas showed the sensitive properties of the sensor for the tested gas.

S5. DSC curves and variable temperature XRD patterns of loose-packed m-$BiVO_4$ nanoellipsoids

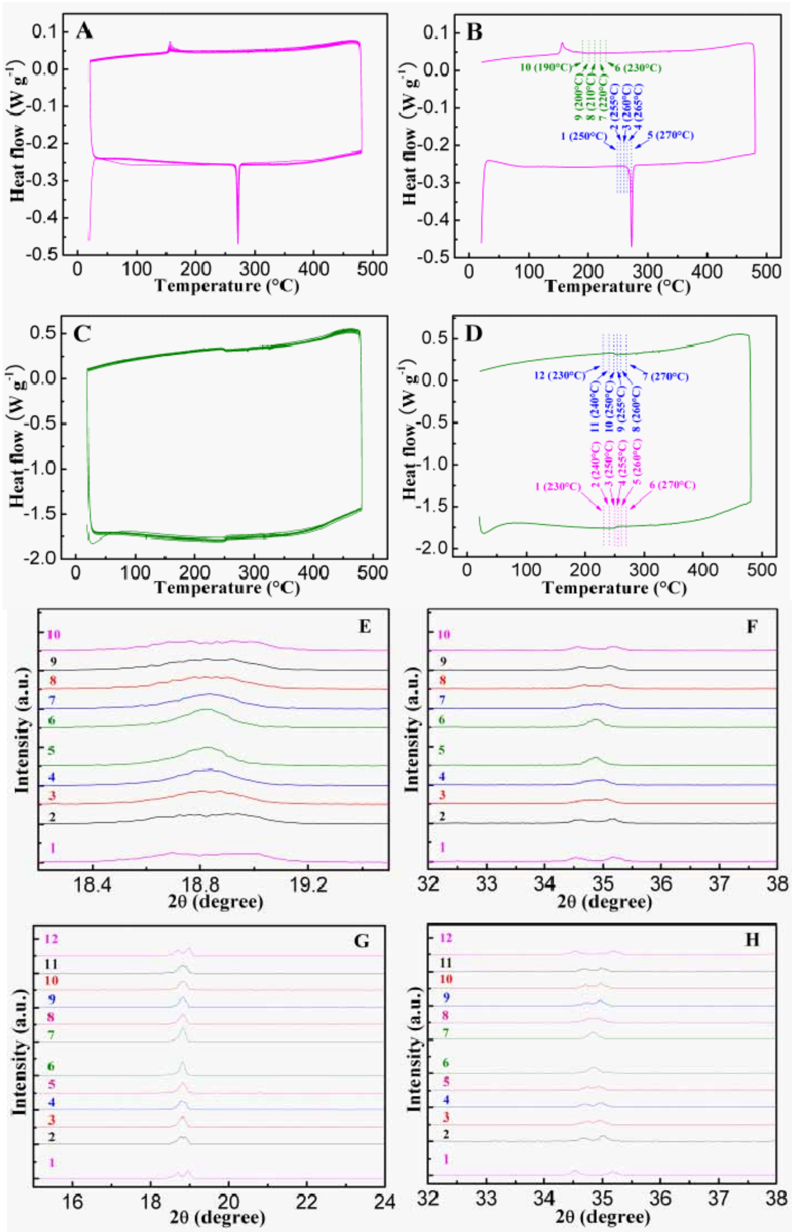

Fig. S4 DSC cycling curves and the corresponding first cycle of ellipsoidal $BiVO_4$ (A, B) and bulk $BiVO_4$ (C, D) with a heating/cooling rate of 10 °C min^{-1} between 20 °C and 480 °C; Enlarged variable temperature XRD patterns of ellipsoidal $BiVO_4$ (E, F) at 250 °C, 255 °C, 260 °C, 265 °C, 270 °C, 230 °C, 220 °C, 210 °C, 200 °C, 190 °C (corresponding to numbers from 1 to 10) and bulk $BiVO_4$ (G, H) at 230 °C, 240 °C, 250 °C, 255 °C, 260 °C, 270 °C, 270 °C, 260 °C, 255 °C, 250 °C, 240 °C, 230 °C (corresponding to numbers from 1 to 12) with a heating/cooling rate of 10 °C min^{-1}, respectively.

The phase change at around the color change temperature of ellipsoidal $BiVO_4$ and bulk $BiVO_4$ was studied by differential scanning calorimetry (DSC) and variable temperature X-ray diffraction (XRD). Thus, as displayed in **Fig. S4A-B** and **C-D** for both $BiVO_4$ products, endothermic and exothermic peaks of DSC curves were observed at around the color change temperature and these peaks had no obvious variations after ten cycles, indicating a good cyclability of $BiVO_4$. Also, one can clearly see that the transformation enthalpies of the ellipsoidal $BiVO_4$ (**Fig. S4A-B**) were much higher than that of bulk $BiVO_4$ (**Fig. S4C-D**), thus possessing more striking color change which was consistent with the above result. Furthermore, compared with the bulk $BiVO_4$, a thermal hysteresis phenomenon was observed in ellipsoidal $BiVO_4$ nanocrystals (**Fig. S4A-B**); meanwhile, their hysteresis width, the difference between the temperatures of maximal endothermic peak during heating (T_{ph}) and maximal exothermic peak during cooling (T_{pc}), is $\Delta T=T_{ph}-T_{pc}=116$ K. In order to further study the phase transformation process of $BiVO_4$ at around the color variation temperature, the variable temperature X-ray diffraction was used to elucidate the structural phase transitions. Then, according to the endothermic and exothermic peaks of the first DSC cycles (**Fig. S4B and D**) resulted from phase change of $BiVO_4$, a series temperature points around peak temperatures such as 250 °C, 255 °C, 260 °C, 265 °C, 270 °C, 230 °C, 220 °C, 210 °C, 200 °C, 190 °C (corresponding to numbers from 1 to 10 in **Fig. S4E-F**) for the ellipsoidal $BiVO_4$ while 230 °C, 240 °C, 250 °C, 255 °C, 260 °C, 270 °C, 270 °C, 260 °C, 255 °C, 250 °C, 240 °C, 230 °C (corresponding to numbers from 1 to 12 in **Fig. S4G-H**) for bulk $BiVO_4$ were performed in order to detailedly elucidate their phase transition processes. As is well known, the peaks, which are split at 2θ = 18.5°, 35°, 46° and 59°, are evidence to differentiate between monoclinic and tetragonal scheelite phase of $BiVO_4$.[3,5,12] Thus, for ellipsoidal $BiVO_4$ as depicted in **Fig. S4E-F**, the peaks of 2θ = 18.5° and 35° gradually changed from obvious split to unsplit when heating from 250 °C to 270 °C, indicating that a gradual phase transformation from the monoclinic to tetragonal phase of $BiVO_4$ had taken place during the heating. Meanwhile, when the temperature decreased from 230 °C to 190 °C, the peaks at 2θ = 18.5° and 35° gradually split from one peak to two peaks, indicating that the t-$BiVO_4$ gradually retransformed to monoclinic phase. Comparatively, as for bulk $BiVO_4$ shown in **Fig. S4G-H**, it progressed the same monoclinic to tetragonal phase transformation process when heating from 230 °C to 270 °C, and then the tetragonal phase could also retransform to monoclinic form when the temperature decreased from 270 °C to 230 °C. In brief, for both ellipsoidal $BiVO_4$ and bulk $BiVO_4$, the phase change process from monoclinic to tetragonal form is a step-by-step process. That is to say, regarding the ellipsoidal $BiVO_4$, the mixed monoclinic and tetragonal phases exist in the temperature ranges of 250 °C-270 °C and 230 °C-190 °C in the heating and cooling processes, respectively; similarly, as to the bulk $BiVO_4$, the mixture of the two phases exist in the temperature ranges of 230 °C-270 °C and 270 °C-230 °C in the heating and cooling processes, respectively. Interestingly, the temperature ranges of mixed phases for ellipsoidal $BiVO_4$ are smaller than those of bulk $BiVO_4$, which means that the ellipsoidal $BiVO_4$ exhibits a faster phase change process which has a potential to indicate temperature more effectively. Furthermore, XRD results, as shown in **Fig. S4E-F**, indicate that the ellipsoidal $BiVO_4$ has thermal hysteresis which is in agreement with the above DSC results (**Fig. S4A-B**).

6. Crystal structure of monoclinic and tetragonal scheelite $BiVO_4$

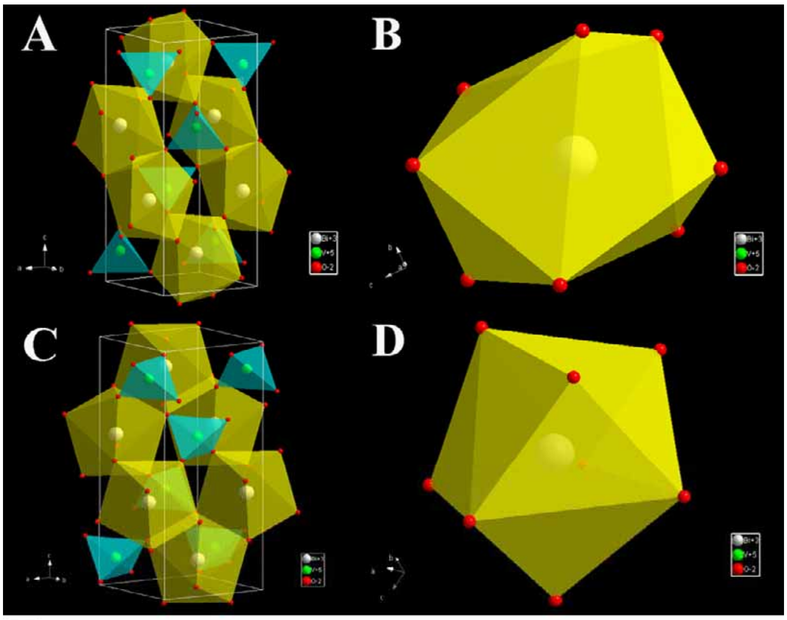

E

crystal system	a	b	c	β	Bi-O (bond length/Å)	V-O (bond length/Å)
monoclinic	5.197	5.096	11.702	90.4	2.3462×2 2.3747×2 2.5279×2 2.6055×2	1.7444×2 1.7475×2
tetragonal	5.105	5.105	11.577	90	2.4726×4 2.3985×4	1.7292×4

Fig. S5 Schematic crystal structure and enlarged Bi-O dodecahedra of monoclinic scheelite $BiVO_4$ (A, B) and tetragonal scheelite $BiVO_4$ (C, D); (E) Cell parameters and bond lengths of $BiVO_4$ with scheelite structure

As is well known, the crystal structure of monoclinic scheelite $BiVO_4$ (**Fig. S5A and 5B**) is similar to that of tetragonal scheelite $BiVO_4$ (**Fig. S5C and 5D**) because they possess the same scheelite structure in which BiO_8 dodecahedra and VO_4 tetrahedra are connected by corner-sharing.[13,14] However, the Bi-O polyhedron in the monoclinic structure is more distortion by a $6s^2$ lone pair of Bi^{3+} than that of tetragonal scheelite $BiVO_4$, due to the difference in the Bi-O bond lengths around the bismuth cation (four distinct Bi-O bond lengths exist in m-$BiVO_4$ while only two distinct Bi-O bond lengths in tetragonal form, see **Fig. S5E**).[4,15,16] Thus, when m-$BiVO_4$ transformed to tetragonal form under heating, the Bi-O bonds and V-O bonds would elongate or shorten to certain values. Consequently, it was noteworthy that the variations in bond lengths accompanied with change in cell parameters from monoclinic form (a = 5.197 Å, b = 5.096 Å, c = 11.702 Å, γ = 90.4°, JCPDS 75-2480) to tetragonal phase (a = 5.105 Å, c = 11.577 Å, JCPDS 78-1534) would result in difference in their band gaps.[12] Then the varied band gaps would lead to different visible light absorption thus taking on diverse colors.

Notes and references

1 M. Gotić, S. Musić, M. Ivanda, M. Šoufek and S. Popović, *J. Mol. Struct.,* 2005, **744**, 535.

2 G. S. Li, D. Q. Zhang and J. C. Yu, *Chem. Mater.,* 2008, **20**, 3983.

3 L. Zhang, D. Chen and X. Jiao, *J. Phys. Chem. B,* 2006, **110**, 2668.

4 A. L. Linsebigler, G. Q. Lu and J. T. Yates, *J. Chem. Rev.,* 1995, **95**, 735.

5 L. Zhou, W. Z. Wang, L. S. Zhang, H. L. Xu and W. Zhu, *J. Phys. Chem. C,* 2007, **111**, 13659.

6 N. Pinna, G. Neri, M. Antonietti and M. Niederberger, *Angew. Chem. Int. Ed.,* 2004, **116**, 4445.

7 N. Pinna, G. Neri, M. Antonietti and M. Niederberger, *Angew. Chem. Int. Ed.,* 2004, **43**, 4345.

8 J. W. Gardner, *Semicond. Sci. Technol.,* 1989, **4**, 345.

9 T. Wolkenstein, *Plenum: New York*, 1991, pp. 35-182.

10 M. H. Cao, Y. D. Wang, T. Chen, M. Antonietti and M. Niederberger, *Chem. Mater.,* 2008, **20**, 5781.

11 P. Lv, Z. A. Tang, J. Yu, F. T. Zhang, G. F. Wei, Z. X. Huang and Y. Hu, *Sensor Actuator B Chem.,* 2008, **132**, 74.

12 S. Tokunaga, H. Kato and A. Kudo, *Chem. Mater.,* 2001, **13**, 4624.

13 D. Barreca, L. E. Depero, V. Di Noto, G. A. Rizzi, L. Sangaletti and E. Tondello, *Chem. Mater.,* 1999, **11**, 255.

14 J. Granzin and D. Pohl, *Z. Kristallogr.,* 1984, **169**, 289.

15 J. Liu, J. Chen and D. Li, *Acta Phys. Sinica,* 1983, **32**, 1053.

16 A. W. Sleight, H. Y. Chen and A. Ferretti, *Mat. Res. Bull.*, 1979, **14**, 1571.